Hindawi
Geofluids
Volume 2022, Article ID 9335126, 17 pages
https://doi.org/10.1155/2022/9335126

Research Article

Coupled Effect of Carbon Nanotubes and Crushing on Shear Strength and Compression of Calcareous Sand Seeped by Colloidal Silica

Weifeng Jin, Ying Tao, and Rongzhong Cheng

School of Civil Engineering and Architecture, Zhejiang University of Science and Technology, Hangzhou 310023, China

Correspondence should be addressed to Weifeng Jin; jinweifenga@163.com

Received 26 January 2022; Revised 28 June 2022; Accepted 6 July 2022; Published 12 August 2022

Academic Editor: Tianshou Ma

Colloidal silica, which has a low viscosity, can seep quickly through sand and subsequently form silica gel to stabilize the sand. The addition of carbon nanotubes can improve the strength of the sand-gel composite. However, previous literature has not investigated the coupled effect of carbon nanotubes and sand crushing on the strength and compression of colloidal-silica-stabilized calcareous sand. So we prepared 86 specimens with 2 different concentrations of colloidal silica and 9 different contents of carbon nanotubes. Then, we performed triaxial shearing and isotropic compression tests based on the triaxial system. The test results show the following: (1) The same carbon nanotube content at the higher concentration of colloidal silica results in higher shear strength, but increasing crushing makes the shear strengths, respectively, caused by 10 wt% and 40 wt% colloidal silica dispersed with carbon nanotubes tend to be the same. (2) The optimal content of carbon nanotubes, which leads to the maximum shear strength, is distributed differently in different concentrations of colloidal silica; i.e., as crushing increases, the optimal carbon nanotube content drifts from 0.03 wt% to 0.10 wt% in 10 wt% colloidal silica, while 40 wt% colloidal silica stabilizes the optimal carbon nanotube content around 0.08 wt%. (3) Compared with carbon nanotubes in 10 wt % colloidal silica, carbon nanotubes in 40 wt% colloidal silica cause higher cohesion rather than internal friction angle, which is the mechanism of higher shear strength at higher colloidal silica concentration with the same carbon nanotube content. (4) For isotropic compression, minimal compression is caused by 40 wt% colloidal silica plus 0.1 wt% carbon nanotubes.

1. Introduction

Colloidal silica, composed of silica nanoparticles repelling each other in an alkaline solution, can seep quickly through sand due to its low viscosity [1, 2]. By adjusting the pH of colloidal silica, after an artificially specified period, silica nanoparticles in colloidal silica can agglomerate to form silica gels to stabilize the sand [3, 4]. Previous studies have investigated the transport behaviors of colloidal silica through porous media. For instance, Agapoulaki and Papadimitriou [5] studied travel distance and the effect of temperature on viscosity-versus-time curves, Saiers et al. [6] performed tests on transport through heterogeneous porous media, Hamderi and Gallagher [7] studied the simulation of optimum coverage, Hamderi et al. [8] studied the numerical model for simulating colloidal silica transport through sand columns, and Hamderi and Gallagher [9] studied the effect of injection rate on the degree of grout penetration. Previous studies have also investigated the mechanical properties of sand seeped and stabilized by colloidal silica; for example, Pamuk et al. [10] performed centrifuge tests on colloidal-silica-stabilized site, Conlee et al. [11] performed centrifuge modeling for liquefaction mitigation, Conlee [12] performed centrifuge model tests and full-scale field tests on colloidal-silica-stabilized soil, Kodaka et al. [13] modeled strength and cyclic deformation characteristics of colloidal-silica-

Table 1: Properties of sand sample.

Specific gravity (G_s)	Max. dry density (kg/m^3)	Min. dry density (kg/m^3)	Relative density	Coefficient of uniformity (C_u)	Coefficient of curvature (C_c)
2.79	1370	1190	0.516	1.9	1.09

stabilized sand, Díaz-Rodríguez et al. [14] used shear tests to investigate the cyclic strength of sand stabilized with colloidal silica, Kakavand and Dabiri [15] and Wong et al. [16] performed shear tests on sandy soil improved by colloidal silica, Gallagher et al. [17] used triaxial tests to investigate the influence of colloidal silica on cyclic undrained behavior of sand, Mollamahmutoglu and Yilmaz [18] used triaxial tests to study pre- and postcyclic strength of colloidal-silica-stabilized sand, Persoff et al. [19] investigated the influence of dilution and contaminants on the strength of colloidal-silica-stabilized sand, Vranna et al. [20] and Pavlopoulou and Georgiannou [21] investigated the monotonic and cyclic behavior of colloidal-silica-stabilized sand, and Triantafyllos et al. [22] studied the strength and dilatancy of colloidal-silica-stabilized sand. Jin [23] investigated the effect of carbon nanotubes on the strength of colloidal-silica-stabilized sand. But these previous studies focused on noncrushable sands.

Calcareous sands, which are more fragile compared with silica sand, are widely distributed in the ocean. Such calcareous sands can be used as the subgrade to support road base and can support piles of offshore or island infrastructures [24]. The difference in this paper is that we study the effect of crushing on the calcareous sand stabilized by carbon-nanotube-dispersed colloidal silica, while previous studies cannot answer how the coupled effect of carbon nanotubes and sand crushing influences the shear strength and compression of colloidal-silica-stabilized calcareous sand. The new contributions of this paper are as follows: We provide the optimal carbon nanotube contents lead to the maximum shear strengths at different colloidal-silica-concentration levels, the mechanism by which the same carbon nanotube content results in different shear strengths at different colloidal silica concentrations, and the optimal combination of colloidal silica and carbon nanotubes that yields minimal compression.

In this paper, based on the triaxial shearing and isotropic compression tests, we explore the coupled effect of carbon nanotube content and sand crushing on the shear strength and compression of colloidal-silica-stabilized calcareous sand. That is, we study the distributions of shear strength and the optimal carbon nanotube content at different colloidal-silica-concentration levels, the mechanism by which the same carbon nanotube content leads to different shear strengths at different colloidal silica concentrations, as well as the combination of colloidal silica and carbon nanotubes that minimizes compression.

2. Experimental Details

2.1. Experimental Materials. The marine calcareous sand used was from the Philippines. Index properties of the sand are listed in Table 1. This calcareous sand is easily breakable,

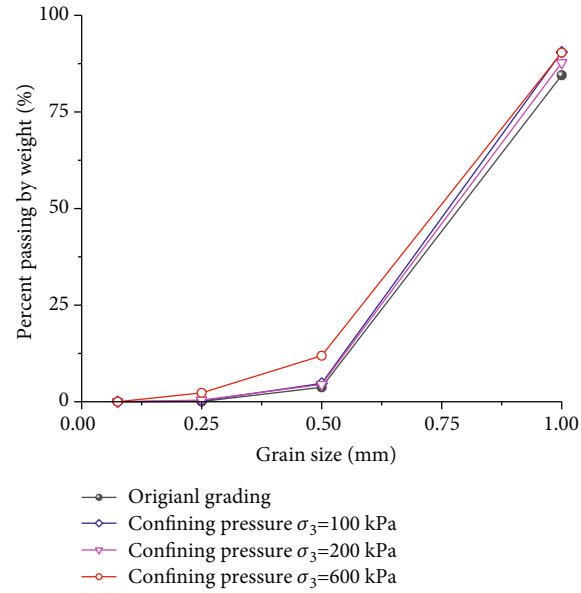

Figure 1: Grain size distribution of unstabilized calcareous sand under different confining pressures in triaxial tests.

and the amount of breakage increases with increasing confining pressure during triaxial tests. The crushable properties of this marine sand were shown by the grain size distribution (GSD) curves before and after the triaxial tests (see Figure 1). Apparently, the amount of breakage increases as the confining pressure increases from 100 kPa to 600 kPa.

The colloidal silica used was provided by Qingdao Maike Silica Gel Dessicant Co., Ltd., and two concentrations of 10% and 40% by weight were used. For colloidal silica, silica nanoparticles are suspended and repel each other under an alkaline environment, with diameter distributions of 10–20 nm. The physical properties of the colloidal silica are shown in Table 2.

The initial multiwalled carbon nanotubes (MWCNTs) were dispersed in deionized water (10 wt %) with a nonionic surfactant, and this solution was produced by Nanjing Xianfeng Nano Material Technology Co., Ltd. We used these MWCNTs as reinforcing fibers. The physical and structural properties of MWCNTs are listed in Table 3. The MWCNTs have inner diameters of 5-15 nm, outer diameters of >50 nm, and lengths of <10 μm. The specific surface area is >230 m^2/g according to the manufacturer.

2.2. Specimen Preparation and Testing Apparatus. Experimental materials, i.e., carbon nanotubes, colloidal silica, and the calcareous sand, are shown in Figure 2(a). Relative density used in Table 1 is the one used for sand in the mold

Table 2: Physical properties of the colloidal silica.

SiO_2 (%)	pH	Density (g/cm^3)	Viscosity (mPa·s)	Average particle size (nm)
10%	8.5~9.5	1.08~1.10	3.0	10~20
40%	9.0	1.28~1.3	25.0	10~20

Table 3: Properties of multiwalled carbon nanotubes.

Inner diameters (nm)	Outer diameter (nm)	Length (μm)	Specific surface area (m^2/g)	Density (g/cm^3)
5-15	>50	<10	>40	2.1

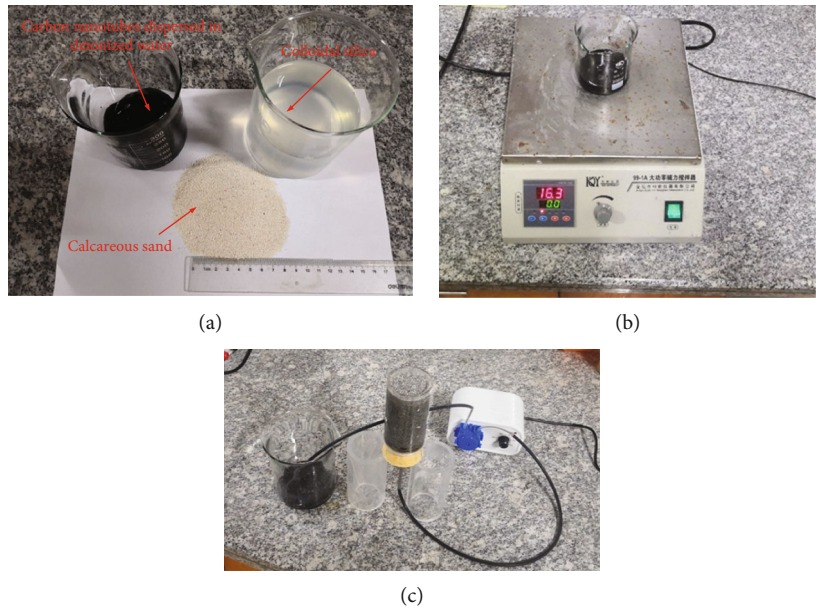

Figure 2: Specimen preparation: (a) experimental materials, (b) magnetically stirred mixture of carbon nanotubes and colloidal silica, and (c) the carbon-nanotube-dispersed colloidal-silica seeped through sand.

before the seepage of colloidal silica. For each specimen, air pluviation method was used; i.e., we used the spoon to pour sand into the mold, and the mass of the sand of each specimen was almost the same, giving the relative density in Table 1. The sand specimens were treated as the following steps: first, the colloidal silica was magnetically stirred with carbon nanotubes for 30 minutes (see Figure 2(b)), and the pH of colloidal silica was adjusted to 5.0-5.5 by adding acetic acid; then, by a peristaltic pump, the carbon-nanotube-dispersed colloidal-silica was slowly injected into the sand from the bottom of a cylindrical mold (see Figure 2(c)).

A GDS- (Geotechnical Digital Systems-) advanced triaxial system (see Figure 3) was used to carry out drained triaxial and isotropic compression tests on specimens. The diameter and height of the test specimen are 38 mm and 76 mm, respectively. During triaxial testing, as shown in Figure 3, the specimen is subjected to the axial stress σ_1 in the vertical direction and the confining pressure σ_3 in the horizontal direction, where σ_3 is set to be constant and $\sigma_1 > \sigma_3$, while for isotropic compression, σ_1 and σ_3 increase simultaneously and we set $\sigma_1 = \sigma_3$.

2.3. Experimental Plan. The experimental plans, as summarized in Tables 4 and 5, are mainly aimed at investigating the coupled effect of the content of carbon nanotube and crushing on the shear strength and isotropic compression property of the stabilized specimens. Sands were seeped and stabilized by the mixture of colloidal silica and carbon nanotubes. The specimens were cured for 3 days before testing. The concentrations of colloidal silica are 10 wt% and 40 wt%, respectively. The contents of carbon nanotubes are 0%, 0.01%, 0.02%, 0.03%, 0.04%, 0.05%, 0.06%, 0.08%, and 0.10% by weight of colloidal silica, respectively.

For the shear strength, drained triaxial compression tests were performed with confining pressures of 100 kPa, 200 kPa, and 600 kPa, respectively (see Table 4). For our drained triaxial shear tests, the axial loading rate was 0.4 mm/min.

While for the isotropic compression property, isotropic compression tests were performed by the triaxial system. That is, the horizontal and vertical stresses on the specimen were set to be equal during each test, and the stresses increased from 100 kPa to 800 kPa, so as to perform the isotropic compression process. We tested two specimens under

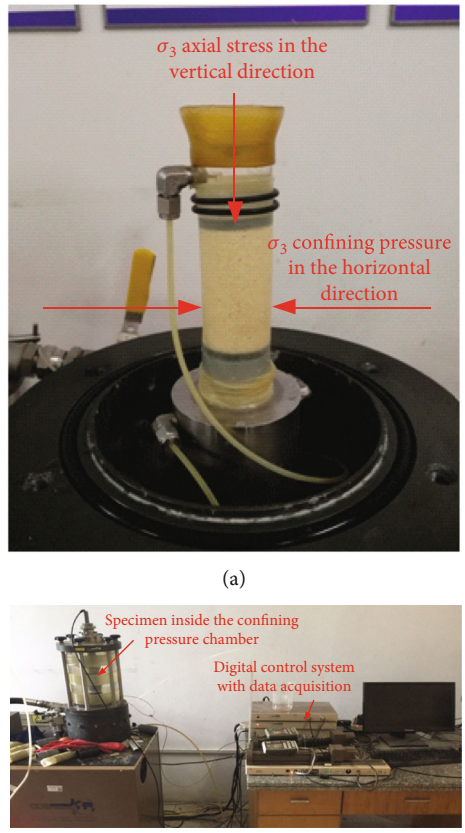

Figure 3: Specimen for triaxial compression test: (a) specimen under axial and confining loads and (b) GDS advanced triaxial system.

Table 4: Experimental plan of drained triaxial compression tests on the strength (54 specimens).

Colloidal silica concentration (wt%)	Curing period (days)	Carbon nanotube content (wt%)	Confining pressure, σ_3 (kPa)
10 and 40	3	0, 0.01, 0.02, 0.03, 0.04, 0.05, 0.06, 0.08, and 0.10	100, 200, and 600

Table 5: Experimental plan of isotropic compression tests (32 specimens).

Colloidal silica concentration (wt%)	Carbon nanotube content (wt%)	Curing period (days)	Starting stress of isotropic compression (kPa)	Ending stress of isotropic compression (kPa)
10 and 40	0.01, 0.02, 0.03, 0.04, 0.05, 0.06, 0.08, and 0.10	3	100	800

the same condition and then took the average to obtain the slope of the isotropic compression line.

Thus, a total of 86 specimens (54 for strength and 32 for isotropic compression) were tested.

3. Testing Results and Analysis

3.1. Coupled Effect of Carbon Nanotubes and Sand Crushing on the Shear Strength. We use the deviatoric stress at failure as shear strength. So we can get the shear strength from the peak point of the curve of deviatoric stress versus axial strain, as shown in the upper graph of Figure 4. The peak deviatoric stress was used as the shear strength for sand stabilized by Portland cement, as presented in the following reference, by Schnaid et al. [25]. So we follow this definition to use the peak deviatoric stress as the shear strength.

For specimen under the axial stress σ_1 and the confining stress σ_3 (see Figure 3(a)), the mean effective stress p and the deviatoric stress q are defined as conventional triaxial variables, as shown below.

$$p = \frac{\sigma_1 + 2\sigma_3}{3}, \tag{1}$$

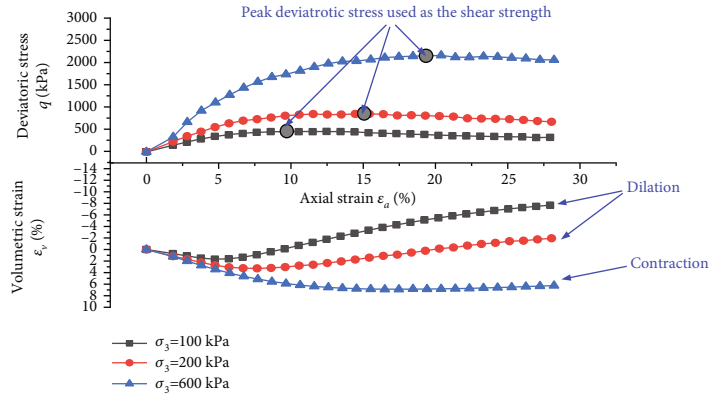

Figure 4: Deviatoric stress versus axial strain and volumetric strain versus axial strain (10 wt%colloidal silica + 0.05 wt%carbon nanotubes).

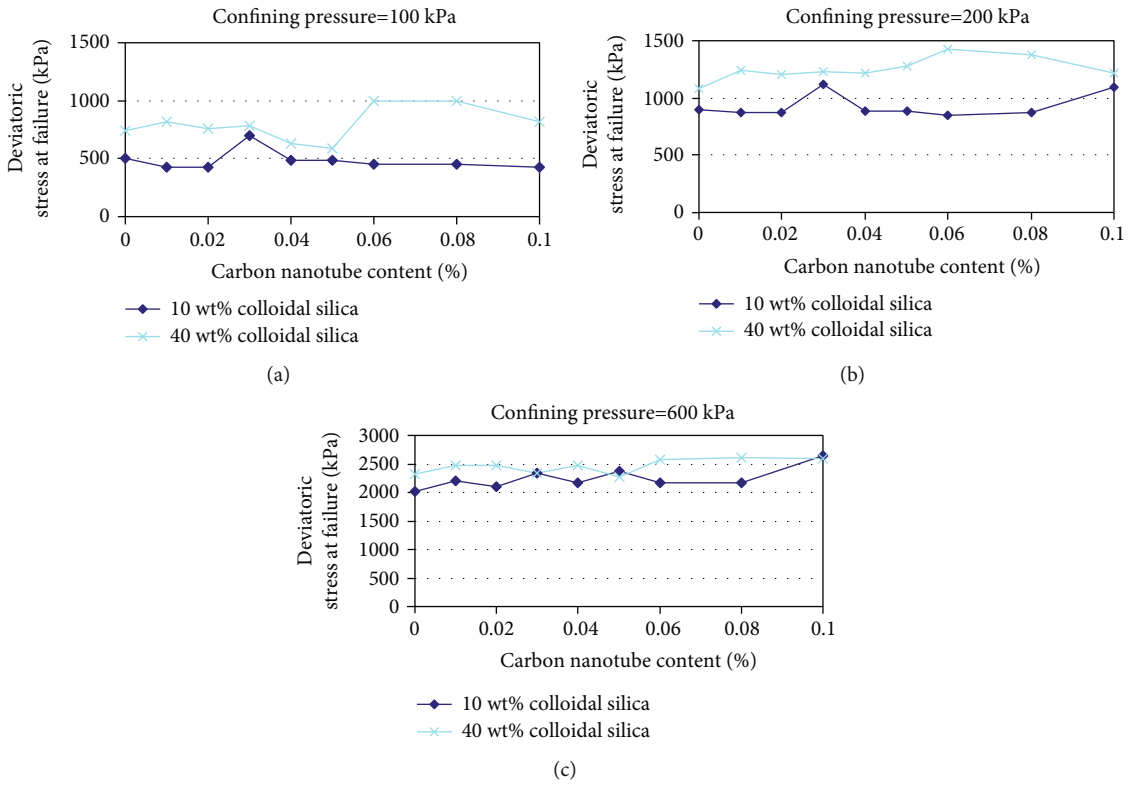

Figure 5: Deviatoric stress at failure vs. carbon nanotube content, and (a) confining pressure = 100 kPa, (b) confining pressure = 200 kPa, and (c) confining pressure = 600 kPa.

$$q = \sigma_1 - \sigma_3. \quad (2)$$

The degree of crushing can be characterized by the confining pressure. Crushing increases with increasing confining pressure, which is proved by previous literatures [26–31]. This confining pressure σ_3, which acts on the specimen in the horizontal direction, is constant for a certain specimen during our triaxial compression test. The bottom graph of Figure 4 shows that the volumetric strain changes with the axial strain. It should be noted that traditionally, for soil mechanics, when the sand specimen contracts, the volumetric strain is set to be positive. So in the case of relatively low confining pressures of 100 kPa and 200 kPa, the volumetric strain first contracts then dilates, indicating that the crushing is relatively small, since such trend of volumetric-strain change is the typical case for noncrushable grains [32–35], or the typical case for few crushing of both noncemented breakable grains [36, 37] and cemented breakable grains [38, 39]. While as the confining pressure increases to 600 kPa, the specimen only exhibits contraction, indicating that crushing is dominant, as shown in the previous literature for non-cemented breakable grains [24, 40–47]

Table 6: Deviatoric stress at failure.

Colloidal silica concentration	Confining pressure (kPa)	Deviatoric stress at failure (kPa)								
		Carbon nanotube 0 wt%	Carbon nanotube 0.01 wt%	Carbon nanotube 0.02 wt%	Carbon nanotube 0.03 wt%	Carbon nanotube 0.04 wt%	Carbon nanotube 0.05 wt%	Carbon nanotube 0.06 wt%	Carbon nanotube 0.08 wt%	Carbon nanotube 0.10 wt%
10 wt%	100	504	423	429	698	484	489	455	448	428
10 wt%	200	898	874	870	1122	889	882	850	879	1093
10 wt%	600	2009	2209	2094	2339	2163	2376	2165	2166	2641
40 wt%	100	744	820	760	786	634	589	993	999	817
40 wt%	200	1088	1241	1207	1227	1220	1282	1431	1373	1213
40 wt%	600	2315	2472	2473	2340	2468	2268	2582	2605	2590

and cemented breakable grains [48]. So here we use the confining pressure as an indicator to approximately describe the degree of crushing.

Since deviatoric stress at failure is used as shear strength, Figures 5(a)–5(c) show the curves of shear strength versus carbon nanotube content under different confining pressures of 100 kPa, 200 kPa, and 600 kPa. The corresponding data are shown in Table 5.

As shown in Figure 5, generally, carbon nanotubes in 40 wt% colloidal silica causes greater shear strength than carbon nanotubes in 10 wt% colloidal silica.

For 10 wt% colloidal silica, the optimal carbon nanotube contents are 0.03 wt%, 0.03 wt%, and 0.10 wt% under the confining pressure of 100 kPa, 200 kPa, and 600 kPa, respectively. Compared with the non-carbon-nanotube-dispersed colloidal-silica-stabilized specimen, under the three different confining pressures, these three optimal carbon nanotube contents result in the maximum strengths by up to 38%, 25%, and 31%, respectively (see Figure 5 and Table 6).

For 40 wt% colloidal silica, the optimal carbon nanotube contents are 0.08 wt%, 0.06 wt%, and 0.08 wt% under the confining pressure of 100 kPa, 200 kPa, and 600 kPa, respectively. Compared with the non-carbon-nanotube-dispersed colloidal-silica-stabilized specimen, these three optimal contents of carbon nanotubes result in the maximum strengths by up to 34%, 32%, and 13% under the three different confining pressures, respectively (see Figure 5 and Table 6). It should be noted that at the confining pressure of 200 kPa, colloidal silica concentrations of 0.06 wt% and 0.08 wt% result in the strengths of 2582 kPa and 2605 kPa, respectively, indicating that the difference between the two strengths is small. So it can be considered that at the confining pressure of 200 kPa, the optimal carbon nanotube content is still around 0.08 wt%.

Therefore, from the perspective of the concentration of colloidal silica, 10 wt% colloidal silica results in the drift of the optimal carbon nanotube content from 0.03 wt% to 0.10 wt% with increasing crushing (namely with increasing confining pressure), while 40 wt% colloidal silica results in a stable optimal carbon nanotube content of 0.08 wt% under different degrees of crushing (namely under different confining pressures). So compared with 10 wt% colloidal silica, 40 wt% colloidal silica not only causes higher strengths of carbon-nanotube-reinforced specimens but also leads to a more stable optimal content of carbon nanotubes under different degrees of crushing.

From the perspective of crushing, as the degree of crushing increases (i.e., the confining pressure increases from 100 kPa to 600 kPa), the two curves of strength versus carbon-nanotube content in 10 wt% and 40 wt% colloidal silica gradually approach each other (see Figure 5). That is, at the confining pressure of 100 kPa, the two curves of strength versus carbon-nanotube content have no intersection (see Figure 5(a)), and the difference in peak strength between 10 wt% and 40 wt% colloidal silica dispersed with carbon nanotubes is 301 kPa (see Table 6), while at the confining pressure of 600 kPa, the two curves of strength versus carbon-nanotube content intersects with each other and the peak strengths, respectively, caused by 10 wt% and 40 wt% colloidal silica reinforced by optimal carbon-nanotube contents nearly coincide. So as the crushing increases (namely the confining pressure increases), the difference in strengths, respectively, caused by 10 wt% and 40 wt% colloidal silica dispersed with carbon nanotubes becomes smaller and smaller. Figure 5 shows that as the degree of crushing increases (i.e., the confining pressure increases from 100 kPa to 600 kPa), the two strength curves with 10 wt% and 40 wt% colloidal silica gradually approach each other. The mechanism is that the competition of bonding and particle crushing leads to this phenomenon. At low confining pressure (100 kPa), bonding is the dominant contributor to strength and particle crushing is small, while carbon-nanotube-dispersed colloidal silica affects bonding, so the two strength curves with different colloidal silica concentrations are significantly different. However, as the confining pressure increases to 600 kPa, the bonding structures are destroyed and particle crushing is dominant, so the strength is mainly determined by particle crushing not bonding, then the difference in colloidal silica has little effect on the strength and the two strength curves approach each other.

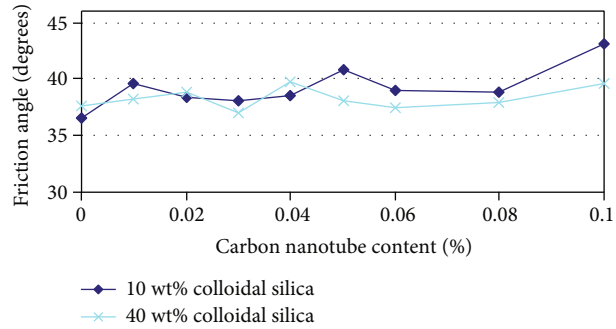

Figure 6: Friction angle vs. carbon nanotube content.

When the crushing is relatively small (at the confining pressures of 100 kPa and 200 kPa), the strength caused by 40 wt% colloidal silica with the optimal carbon-nanotube content is obviously greater than that caused by 10 wt% colloidal silica with the optimal carbon-nanotube content; while the increase of crushing can increasingly erase the peak strength difference between 10 wt% and 40 wt% colloidal silica with optimal carbon-nanotube contents, especially when crushing is dominant (at the confining pressure of 600 kPa), the peak strengths, respectively, caused by 10 wt% and 40 wt% colloidal silica with optimal carbon-nanotube contents are almost the same. So for the strengths under different concentrations of colloidal silica dispersed with carbon nanotubes, although the reinforcing effect of carbon nanotubes in 40 wt% colloidal silica is better than that of carbon nanotubes in 10 wt% colloidal silica, as the crushing increases, the difference between the reinforcing effects of the two gradually decreases.

Figure 6 shows the curves of internal friction angle versus carbon nanotube content, and the corresponding data are shown in Table 7. Figure 6 demonstrates that though carbon nanotubes enhance the internal friction angle,

Table 7: Internal friction angle.

Colloidal silica concentration	Internal friction angle (deg)								
	Carbon nanotube 0 wt%	Carbon nanotube 0.01 wt%	Carbon nanotube 0.02 wt%	Carbon nanotube 0.03 wt%	Carbon nanotube 0.04 wt%	Carbon nanotube 0.05 wt%	Carbon nanotube 0.06 wt%	Carbon nanotube 0.08 wt%	Carbon nanotube 0.10 wt%
10 wt%	36.58	39.57	38.31	38.09	38.57	40.76	38.94	38.91	43.04
40 wt%	37.55	38.22	38.81	37.03	39.75	38.02	37.45	37.85	39.60

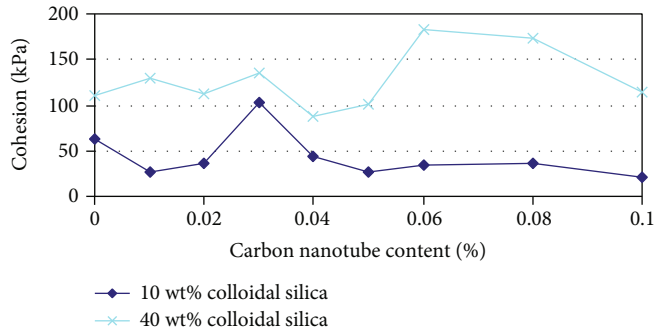

Figure 7: Cohesion vs. carbon nanotube content.

carbon nanotubes in 10 wt% colloidal silica have almost the same effect on the internal friction angle as they in 40 wt% colloidal silica, indicating that the reinforcing difference between 10 wt% and 40 wt% colloidal silica dispersed with carbon nanotubes does not depend on the internal friction angle.

Figure 7 shows the curves of cohesion versus carbon nanotube content, and the corresponding data are shown in Table 8. Figure 7 shows that carbon nanotubes in 40 wt% colloidal silica cause significantly higher cohesion than carbon nanotubes in 10 wt% colloidal silica. So the reason why carbon nanotubes in 40 wt% colloidal silica result in relatively higher strength than carbon nanotubes in 10 wt% colloidal silica is that 40 wt% colloidal silica is more helpful for carbon nanotubes to enhance strength by increasing cohesion rather than internal friction angle. The graphs of failure line are shown in Figure 8, and these failure lines (i.e., strength envelops) are linear.

To sum up, carbon nanotubes in 40 wt% colloidal silica better enhance the strength than carbon nanotubes in 10 wt% colloidal silica, whose mechanism is that 40 wt% colloidal silica let carbon nanotubes significantly enhance greater cohesion rather than internal friction angle. In addition, for the maximum strength caused by the optimal carbon nanotube content, as crushing increases (i.e., as confining pressure increases from 100 kPa to 600 kPa), 10 wt% colloidal silica results in the drift of optimal carbon nanotube content from 0.03 wt% to 0.1 wt%, while 40 wt% colloidal silica stabilizes the optimal carbon nanotube content around 0.08 wt%. However, as crushing increases, the strength difference between specimens, respectively, stabilized by 40 wt% and 10 wt% colloidal silica dispersed with carbon nanotubes becomes smaller and smaller.

3.2. Isotropic Compression. For isotropic compression, we applied equal three-dimensional stresses on the cylindrical specimen (as shown in Figure 3, the axial stress σ_1 and the confining pressure σ_3 were set equal), and the stresses increased simultaneously from 100 kPa to 800 kPa. Then, we obtained the relationship between the void ratio e and the mean effective stress p in the e-In(p) plane, as shown in Figure 9. For the same colloidal-silica concentration and carbon-nanotube content, we prepared two specimens and performed two parallel tests to obtain the average slope λ of the compression line. It should be noted that the void ratio e is a nonlinear function of In(p), but to simplify the comparison between different colloidal-silica concentrations and carbon-nanotube contents, we used a linear line to fit the experimental points in the e-$\log_{10}(p)$ plane as the approximate compression line (see Figure 9). We used the least squares method to best fit λ in Equation (3) (see Figure 9). This approximate compression line is defined as follows.

$$e = \Gamma - \lambda \cdot \mathrm{In}(p), \tag{3}$$

where Γ and λ are parameters of the approximate compression line (see Figure 9). We used the slope of the compression line, λ, to compare the effects of different colloidal-silica concentrations and carbon-nanotube contents on the isotropic compression. Obviously, higher λ means easier compression.

The specimen showing minimum compression was stabilized by 40 wt% colloidal silica plus 0.1 wt% carbon nanotubes (see the least slope λ in Figure 10 and Table 9). Figure 10 shows that the slope of the compression line, λ, caused by carbon nanotubes in 10 wt% colloidal silica is greater than that caused by carbon nanotubes in 40 wt% colloidal silica, which means that carbon nanotubes leads to less compression in higher concentration of colloidal silica.

4. Discussion of the Mechanism of the Test Results

Based on our tests, we found that the same carbon nanotube content results in higher shear strength in higher concentration of colloidal silica. But as the confining pressure increases, the two strength curves approaches each other, as shown in Figure 5. The mechanism is that higher concentration of colloidal silica provides higher bonding which leads to higher strength, but as the degree of crushing increases (i.e., the confining pressure increases), the bonding structures are destroyed and particle crushing is dominant. When the effect of particle crushing overwhelms the effect of bonding, the difference in colloidal silica concentration

Table 8: Cohesion.

Colloidal silica concentration	Cohesion (kPa)								
	Carbon nanotube 0 wt%	Carbon nanotube 0.01 wt%	Carbon nanotube 0.02 wt%	Carbon nanotube 0.03 wt%	Carbon nanotube 0.04 wt%	Carbon nanotube 0.05 wt%	Carbon nanotube 0.06 wt%	Carbon nanotube 0.08 wt%	Carbon nanotube 0.10 wt%
10 wt%	63.31	27.10	36.88	102.21	44.52	27.51	33.75	35.94	21.06
40 wt%	109.81	130.35	113.01	135.05	88.17	101.60	181.99	172.73	114.01

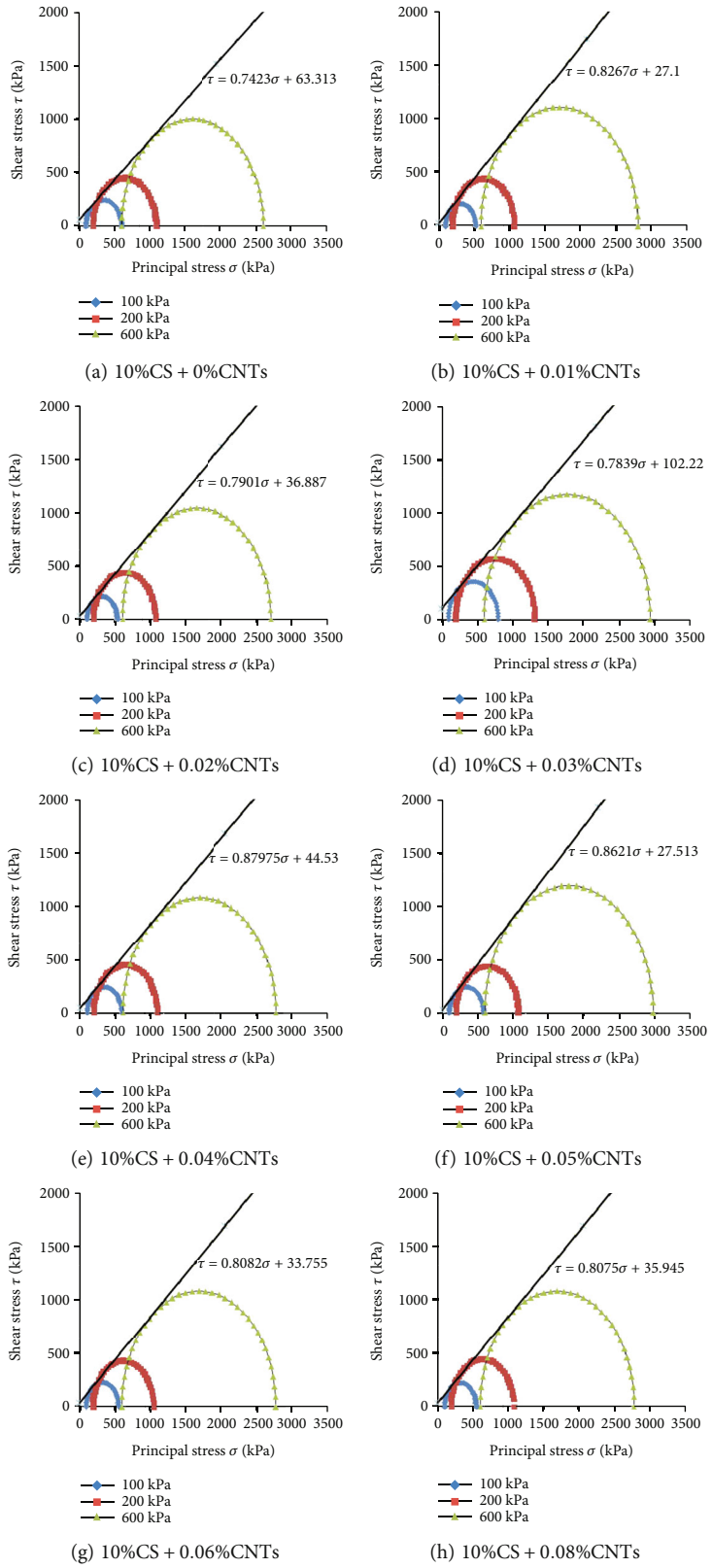

Figure 8: Continued.

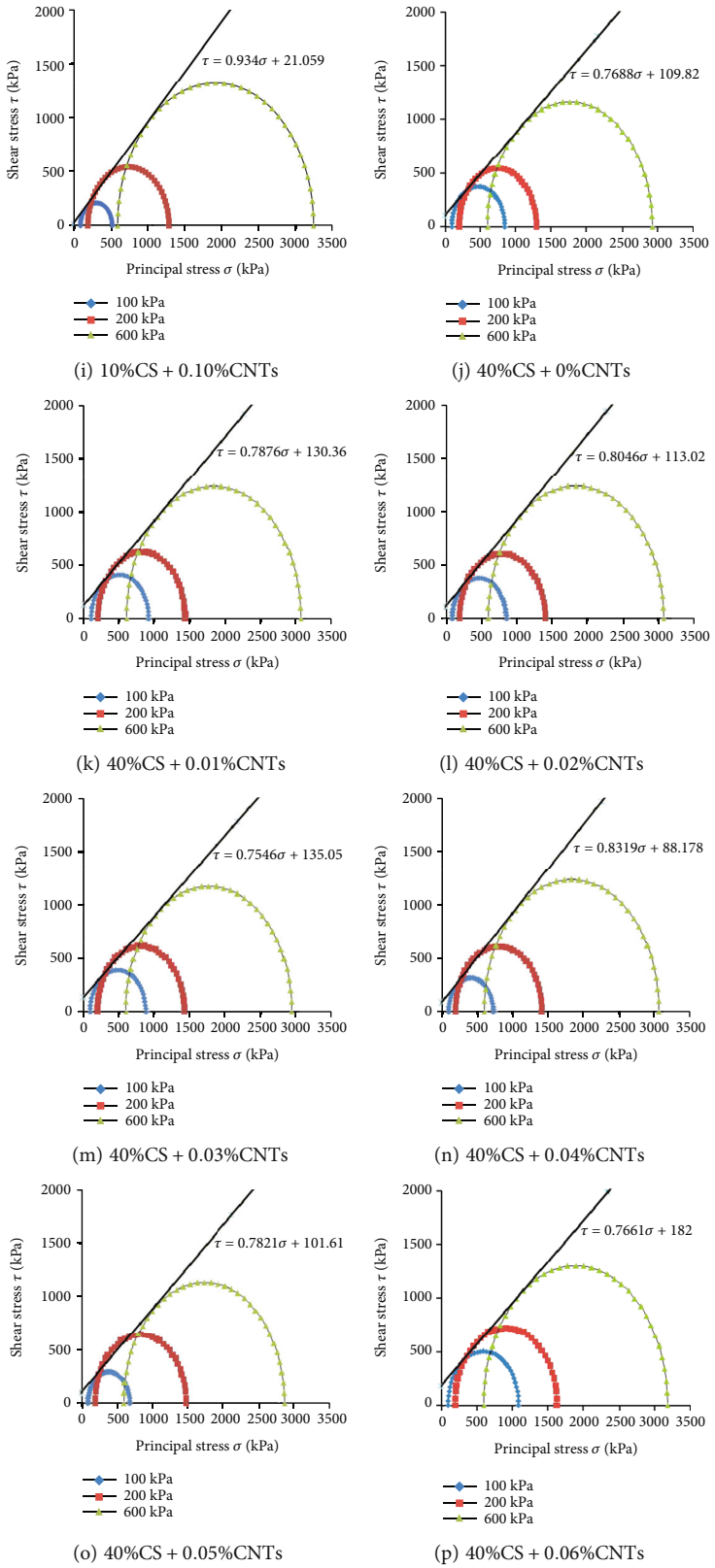

Figure 8: Continued.

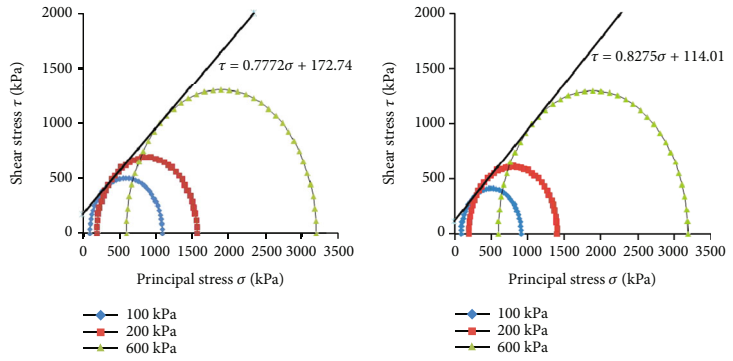

(q) 40%CS + 0.08%CNTs (r) 40%CS + 0.10%CNTs

Figure 8: Strength envelopes. CS: colloidal silica; CNTs: carbon nanotubes.

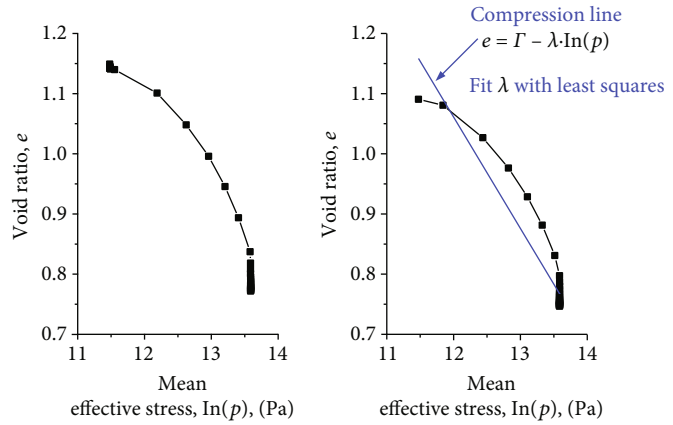

Figure 9: Two parallel isotropic compression tests on the stabilized specimens (10 wt%colloidal silica + 0.02 wt%carbon nanotubes).

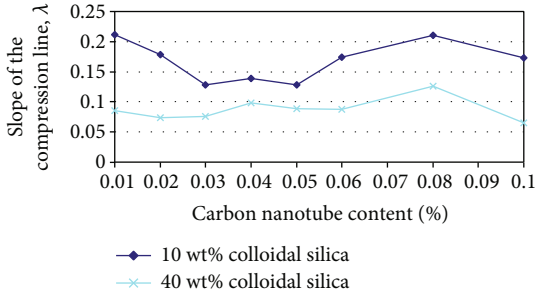

Figure 10: Slope of the isotropic compression line vs. carbon nanotube content.

has little effect on the strength, which means increasing crushing increasingly eliminate the difference in colloidal silica concentration and the two strength curves gradually approaches each other.

For the optimal carbon nanotube content which leads to the maximum strength, we found that 10% colloidal silica causes the optimal carbon nanotube content to drift from 0.03 wt% to 0.10 wt% as particle crushing increases, while 40 wt% colloidal silica stabilizes the optimal carbon nanotube content around 0.08% with increasing crushing. The most intuitive mechanism is that 40 wt% colloidal silica produces more silica gels in the voids between the sand particles, which causes the optimal content of carbon nanotubes to be stable with increasing particle crushing; while 10 wt% colloidal silica produces less silica gels in the voids, which causes the optimal content of carbon nanotubes to drift with increasing crushing. But why filling the voids with more silica gels can stabilize the optimal content of carbon nanotubes still needs to be explored.

It should be noted that at high confining pressure (600 kPa), it does look like scattering for the shear strengths (see Figure 5(c)). But peak strengths are apparent at low confining pressures (i.e., 100 kPa and 200 kPa), as shown in Figures 5(a-b), so it is reasonable to pick up the optimal carbon nanotube content leading to the peak strength at low confining pressures (i.e., 100 kPa and 200 kPa). Therefore, optimal carbon nanotube content can be picked up at low confining pressures (i.e., 100 kPa and 200 kPa), but picking up this optimal content may not be appropriate at high confining pressure (600 kPa). The mechanism of the above phenomenon is that: At low confining pressures (i.e., 100 kPa and 200 kPa), bonding is dominant, so optimal carbon nanotube leading to the peak strength can be picked up; while at high confining pressure (600 kPa), the effect of particle crushing overwhelms the

Table 9: Slope of the isotropic compression line in the plane of void ratio against mean stress.

Colloidal Silica Concentration	Slope of the isotropic compression line, λ							
	Carbon nanotube 0.01 wt%	Carbon nanotube 0.02 wt%	Carbon nanotube 0.03 wt%	Carbon nanotube 0.04 wt%	Carbon nanotube 0.05 wt%	Carbon nanotube 0.06 wt%	Carbon nanotube 0.08 wt%	Carbon nanotube 0.10 wt%
10 wt%	0.212	0.178	0.128	0.139	0.128	0.174	0.210	0.173
40 wt%	0.085	0.074	0.076	0.098	0.089	0.088	0.126	0.065

effect of bonding, and the difference in carbon nanotube content has little effect on the strength, which means increasing crushing increasingly eliminate the difference in carbon nanotube content and an optimal carbon nanotube is not appropriate at high confining pressure.

Compared with 10 wt% colloidal silica, for stabilized sand, 40 wt% colloidal silica makes carbon nanotubes increase more cohesion but has little effect on the internal friction angle, which is the mechanism of higher strength at higher colloidal silica concentration with the same carbon nanotube content.

5. Conclusions

The study of the coupled effect of carbon nanotubes and crushing on the colloidal-silica-stabilized calcareous sand has allowed the authors to establish the following conclusions:

(1) The same carbon nanotube content results in higher shear strength in higher concentration of colloidal silica. However, increasing crushing can increasingly eliminate the difference between peak shear strengths, respectively, caused by 10 wt% and 40% colloidal silica dispersed with carbon nanotubes. Especially when crushing is dominant, the peak shear strengths, which are, respectively, caused by 10 wt% and 40 wt% colloidal silica dispersed with carbon nanotubes, are nearly the same

(2) There exists an optimal carbon nanotube content resulting in maximum shear strength. However, as the degree of crushing increases, different concentrations of colloidal silica lead to different distributions of optimal carbon nanotube content. That is, in 10 wt% colloidal silica, as crushing increases, the optimal carbon nanotube content drifts from 0.03 wt% to 0.10 wt%. On the contrary, 40 wt% colloidal silica stabilizes the optimal carbon nanotube content around 0.08% with increasing crushing

(3) The mechanism by which carbon nanotubes in 40 wt% colloidal silica causes higher shear strength than that in 10 wt % colloidal silica is that, 40 wt% colloidal silica makes carbon nanotubes significantly increase the cohesion rather than the internal friction angle

(4) For isotropic compression, 40 wt% colloidal silica plus 0.1 wt% carbon nanotubes results in minimal compression. In addition, the same carbon nanotube content in a higher concentration of colloidal silica causes less compression

The present work is helpful to the ground stabilization of crushable calcareous sand. That is, in order to maximize the shear strength, when we choose 10 wt% colloidal silica, we need to choose the corresponding carbon nanotube content according to the stress level, such as 0.03 wt% carbon nanotubes at 100 kPa and 200 kPa, or 0.1 wt% at 600 kPa. Conversely, when we choose 40 wt% colloidal silica, we can choose 0.08 wt% carbon nanotubes regardless of stress level. In addition, when we are mainly concerned about the minimal compression for engineering practice, we can choose 40 wt% colloidal silica plus 0.1 wt% carbon nanotubes. However, it should be noted that as the grain size distribution of sand varies, the present results may not be applicable. Under different grain size distributions, the trends of strength and isotropic compression versus carbon nanotube content need to be further explored.

Data Availability

All the data used to support the findings of this study are included within the article.

Conflicts of Interest

The authors declare that they have no conflicts of interest.

Acknowledgments

This research was supported by Zhejiang Provincial Natural Science Foundation of China under Grant No. LHY19E090001 and the National Natural Science Foundation of China under Grant No. 51408547.

References

[1] P. M. Gallagher and Y. Lin, "Colloidal silica transport through liquefiable porous media," *Journal of Geotechnical and Geoenviromental Engineering*, vol. 135, no. 11, pp. 1702–1712, 2009.

[2] P. M. Gallagher, C. T. Conlee, and K. M. Rollins, "Full-scale field testing of colloidal silica grouting for mitigation of liquefaction risk," *Journal of Geotechnical and Geoenviromental Engineering*, vol. 133, no. 2, pp. 186–196, 2007.

[3] Y. Fujita and M. Kobayashi, "Transport of colloidal silica in unsaturated sand: effect of charging properties of sand and silica particles," *Chemosphere*, vol. 154, pp. 179–186, 2016.

[4] P. M. Gallagher, A. Pamuk, and T. Abdoun, "Stabilization of liquefiable soils using colloidal silica grout," *Journal of Materials in Civil Engineering*, vol. 19, no. 1, pp. 33–40, 2007.

[5] G. I. Agapoulaki and A. G. Papadimitriou, "Rheological properties of colloidal silica grout for passive stabilization against liquefaction," *Journal of Materials in Civil Engineering*, vol. 30, no. 10, p. 04018251, 2018.

[6] J. E. Saiers, G. M. Hornberger, and C. Harvey, "Colloidal silica transport through structured, heterogeneous porous media," *Journal of Hydrology*, vol. 163, no. 3-4, pp. 271–288, 1994.

[7] M. Hamderi and P. M. Gallagher, "An optimization study on the delivery distance of colloidal silica," *Scientific Research and Essays*, vol. 8, pp. 1314–1323, 2013.

[8] M. Hamderi, P. M. Gallagher, and Y. Lin, "Numerical model for colloidal silica injected column tests," *Vadose Zone Journal*, vol. 13, no. 2, pp. 1–6, 2014.

[9] M. Hamderi and P. M. Gallagher, "Pilot-scale modeling of colloidal silica delivery to liquefiable sands," *Soils and Foundations*, vol. 55, no. 1, pp. 143–153, 2015.

[10] A. Pamuk, P. M. Gallagher, and T. F. Zimmie, "Remediation of piled foundations against lateral spreading by passive site stabilization technique," *Soil Dynamics and Earthquake Engineering*, vol. 27, no. 9, pp. 864–874, 2007.

[11] C. T. Conlee, P. M. Gallagher, R. W. Boulanger, and R. Kamai, "Centrifuge modeling for liquefaction mitigation using colloidal silica stabilizer," *Journal of Geotechnical and Geoenviromental Engineering*, vol. 138, no. 11, pp. 1334–1345, 2012.

[12] C. T. Conlee, *Dynamic Properties of Colloidal Silica Soils Using Centrifuge Model Tests and a Full-Scale Field Test. Ph.D. Thesis*, Drexel University, Philadelphia, PA, USA, 2010.

[13] T. Kodaka, F. Oka, Y. Ohno, T. Takyu, and N. Yamasaki, "Modeling of cyclic deformation and strength characteristics of silica treated sand," *Geomechanics: Testing, modeling, and simulation, Geotechnical Special Publication No.*, vol. 143, pp. 205–216, 2005.

[14] J. A. Díaz-Rodríguez, V. M. Antonio-Izarraras, P. Bandini, and J. A. López-Molina, "Cyclic strength of a natural liquefiable sand stabilized with colloidal silica grout," *Canadian Geotechnical Journal*, vol. 45, no. 10, pp. 1345–1355, 2008.

[15] A. Kakavand and R. Dabiri, "Experimental study of applying colloidal nano silica in improving sand-silt mixtures," *Int. J. Nano Dimens.*, vol. 9, pp. 357–373, 2018.

[16] C. Wong, M. Pedrotti, G. El Mountassir, and R. J. Lunn, "A study on the mechanical interaction between soil and colloidal silica gel for ground improvement," *Engineering Geology*, vol. 243, pp. 84–100, 2018.

[17] P. M. Gallagher and J. K. Mitchell, "Influence of colloidal silica grout on liquefaction potential and cyclic undrained behavior of loose sand," *Soil Dynamics and Earthquake Engineering*, vol. 22, no. 9-12, pp. 1017–1026, 2002.

[18] M. Mollamahmutoglu and Y. Yilmaz, "Pre- and post-cyclic loading strength of silica-grouted sand," *Geotechnical Engineering*, vol. 163, no. 6, pp. 343–348, 2010.

[19] P. Persoff, J. Apps, G. Moridis, and J. M. Whang, "Effect of dilution and contaminants on sand grouted with colloidal silica," *Journal of Geotechnical and Geoenviromental Engineering*, vol. 125, no. 6, pp. 461–469, 1999.

[20] A. Vranna, T. Tika, and A. Papadimitriou, "Laboratory investigation into the monotonic and cyclic behaviour of a clean sand stabilised with colloidal silica," *Géotechnique.*, vol. 72, no. 5, pp. 377–390, 2022.

[21] E. E. Pavlopoulou and V. N. Georgiannou, "Effect of colloidal silica aqueous gel on the monotonic and cyclic response of sands," *Journal of Geotechnical and Geoenviromental Engineering*, vol. 147, no. 11, p. 04021122, 2021.

[22] P. K. Triantafyllos, V. N. Georgiannou, E. Pavlopoulou, and Y. F. Dafalias, "Strength and dilatancy of sand before and after stabilisation with colloidal-silica gel," *Géotechnique.*, vol. 72, no. 6, pp. 471–485, 2022.

[23] W. F. Jin, Y. Tao, X. Wang, and Z. Gao, "The effect of carbon nanotubes on the strength of sand seeped by colloidal silica in triaxial testing," *Materials.*, vol. 14, no. 20, p. 6119, 2021.

[24] Y. Wu, N. Li, X. Wang et al., "Experimental investigation on mechanical behavior and particle crushing of calcareous sand retrieved from South China Sea," *Engineering Geology*, vol. 280, article 105932, 2021.

[25] F. Schnaid, P. D. M. Prietto, and N. C. Consoli, "Characterization of cemented sand in triaxial compression," *Journal of Geotechnical and Geoenviromental Engineering*, vol. 127, no. 10, pp. 857–868, 2001.

[26] G. Alvarado, N. Lui, and M. R. Coop, "Effect of fabric on the behaviour of reservoir sandstones," *Canadian Geotechnical Journal*, vol. 49, no. 9, pp. 1036–1051, 2012.

[27] M. Cecconi, A. DeSimone, C. Tamagnini, and M. B. A. Viggiani Giulia, "A constitutive model for granular materials with grain crushing and its application to a pyroclastic soil," *International Journal for Numerical and Analytical Methods in Geomechanics*, vol. 26, no. 15, pp. 1531–1560, 2002.

[28] M. B. Cil, R. C. Hurley, and L. Graham-Brady, "Constitutive model for brittle granular materials considering competition between breakage and dilation," *Journal of Engineering Mechanics*, vol. 146, no. 1, p. 04019110, 2020.

[29] A. Daouadji and P.-Y. Hicher, "An enhanced constitutive model for crushable granular materials," *International Journal for Numerical and Analytical Methods in Geomechanics*, vol. 34, no. 6, pp. 555–580, 2010.

[30] C. A. Davy, M. D. Bolton, and N. A. Fleck, "The shearing behaviour of a sugar aggregate," *Acta Materialia*, vol. 52, no. 12, pp. 3587–3601, 2004.

[31] M. E. Kan and H. A. Taiebat, "A bounding surface plasticity model for highly crushable granular materials," *Soils and Foundations*, vol. 54, no. 6, pp. 1188–1201, 2014.

[32] R. Fu, M. R. Coop, and X. Q. Li, "The mechanics of a compressive sand mixed with Tyre rubber," *Géotechnique Letters*, vol. 4, no. 3, pp. 238–243, 2014.

[33] R. Fu, M. R. Coop, and X. Q. Li, "Influence of particle type on the mechanics of sand–rubber mixtures," *Journal of Geotechnical and Geoenviromental Engineering*, vol. 143, no. 9, p. 04017059, 2017.

[34] P. Guo and X. Su, "Shear strength, interparticle locking, and dilatancy of granular materials," *Canadian Geotechnical Journal*, vol. 44, no. 5, pp. 579–591, 2007.

[35] S. A. Harehdasht, M. Karray, M. N. Hussien, and M. Chekired, "Influence of particle size and gradation on the stress-dilatancy behavior of granular materials during drained triaxial compression," *International Journal of Geomechanics*, vol. 17, no. 9, p. 04017077, 2017.

[36] S. H. He, H. F. Shan, T. D. Xia, Z. J. Liu, Z. Ding, and F. Xia, "The effect of temperature on the drained shear behavior of calcareous sand," *Acta Geotechnica*, vol. 16, no. 2, pp. 613–633, 2021.

[37] M. Liu and Y. Gao, "Constitutive modeling of coarse-grained materials incorporating the effect of particle breakage on critical state behavior in a framework of generalized plasticity," *International Journal of Geomechanics*, vol. 17, no. 5, article 04016113, 2017.

[38] M. J. Cui, J. J. Zheng, J. Chu, C. C. Wu, and H. J. Lai, "Bio-mediated calcium carbonate precipitation and its effect on the shear behaviour of calcareous sand," *Acta Geotechnica*, vol. 16, no. 5, pp. 1377–1389, 2021.

[39] M. J. Cui, J. J. Zheng, B. K. Dahal, H. J. Lai, Z. F. Huang, and C. C. Wu, "Effect of waste rubber particles on the shear behaviour of bio-cemented calcareous sand," *Acta Geotechnica*, vol. 16, no. 5, pp. 1429–1439, 2021.

[40] M. Kikumoto, D. M. Wood, and A. Russell, "Particle crushing and deformation behaviour," *Soils and Foundations*, vol. 50, no. 4, pp. 547–563, 2010.

[41] H. Liu, D. Zou, and J. Liu, "Constitutive modeling of dense gravelly soils subjected to cyclic loading," *International Journal for Numerical and Analytical Methods in Geomechanics*, vol. 38, no. 14, pp. 1503–1518, 2014.

[42] J. M. Liu, D. G. Zou, X. J. Kong, and H. B. Liu, "Stress-dilatancy of Zipingpu gravel in triaxial compression tests," *Science China Technological Sciences*, vol. 59, no. 2, pp. 214–224, 2015.

[43] M. Liu, Y. Zhang, and H. Zhu, "3D elastoplastic model for crushable soils with explicit formulation of particle crushing," *Journal of Engineering Mechanics*, vol. 143, no. 12, p. 04017140, 2017.

[44] Z. Wang, G. Wang, and G. Ye, "A constitutive model for crushable sands involving compression and shear induced particle breakage," *Computers and Geotechnics*, vol. 126, article 103757, 2020.

[45] Y. Wu and H. Yamamoto, "Numerical investigation on the reference crushing stress of granular materials in triaxial compression test," *Periodica Polytechnica Civil Engineering*, vol. 59, no. 4, pp. 465–474, 2015.

[46] Y. Xiao, H. L. Liu, Y. M. Chen, J. Jiang, and W. Zhang, "Testing and modeling of the state-dependent behaviors of rockfill material," *Computers and Geotechnics*, vol. 61, pp. 153–165, 2014.

[47] J. Zhang and M. Luo, "Dilatancy and critical state of calcareous sand incorporating particle breakage," *International Journal of Geomechanics*, vol. 20, no. 4, article 04020030, 2020.

[48] M. R. Coop and J. H. Atkinson, "The mechanics of cemented carbonate sands," *Géotechnique*, vol. 43, no. 1, pp. 53–67, 1993.